

Development of a species-specific model of cerebral hemodynamics

SILVIA DAUN^{†*} and THORSTEN TJARDES[‡]

[†]Department of Mathematics, University of Cologne, Weyertal 86-90, Cologne D-50931, Germany

[‡]Department of Trauma and Orthopaedic Surgery, University of Witten-Herdecke, Merheim Medical Center, Ostmerheimerstr. 200, Cologne D-51109, Germany

(Received 23 February; revised 5 July 2005; accepted 27 October 2005)

In this paper, a mathematical model for the description of cerebral hemodynamics is developed. This model is able to simulate the regulation mechanisms working on the small cerebral arteries and arterioles, and thus to adapt dynamically the blood flow in brain. Special interest is laid on the release of catecholamines and their effect on heart frequency, cardiac output and blood pressure. Therefore, this model is able to describe situations of severe head injuries in a very realistic way.

Keywords: Cerebral hemodynamics; Regulation mechanisms; Catecholamines; Cardiac output

1. Introduction

Cerebral perfusion is a critical parameter in many clinical situations, e.g. cerebral infarction or head injury. Many of these conditions have been investigated extensively in experimental and clinical studies with respect to a wide variety of clinical and physiological parameters. In the past decades, the key mechanisms involved in the regulation of cerebral perfusion have been identified. However, it is a well-known problem of classical reductionist-experimental approaches that different physiological parameters cannot be evaluated simultaneously. Consequently, there is very little knowledge concerning the *in-situ* consequences of interactions between different physiological regulatory systems. The therapeutic interventions based on single parameter mechanisms, e.g. hyperventilation to reduce arterial $p\text{CO}_2$, have not proven successful as “single-agent” therapy to improve the outcome in head injured patients. Physiologic data from patients in a clinical context are difficult to obtain as these patients are often in a life threatening condition. Given the high degree of susceptibility of traumatic brain injuries to any external stimuli extensive interventions for data acquisition are ethically questionable as these interventions might affect the outcome. Data collection in healthy control groups is even more problematic with respect to possible complications due to the highly invasive nature of measurement technology. Additionally, the varying extend of traumatic brain injury, comorbidities or additional injuries result in

very heterogeneous patient populations, i.e. the data pool for modelling will be the sum total of very different clinical entities that might display differing behaviour. Mathematical approaches do not suffer from these intrinsic problems. In the past different mathematical models of the cerebral circulation or distinct parts of the regulatory systems have been developed. However, the two major drawbacks of these models are a lack of anatomical coherence and the missing species specificity. For these reasons it has been difficult to validate these models experimentally. Consequently, the ultimate aim of all modelling approaches in clinical medicine, i.e. to arrive at a level of understanding of physiological processes sufficiently profound to derive rules to influence the *in-vivo* system systematically (i.e. therapeutically), has not yet been reached. The model presented in this paper is, therefore, strictly species specific as almost exclusively data from experiments with Sprague-Dawley rats have been used for parameter estimation. To facilitate the experimental validation, as well as model based experimental interventions the structure of the model is kept very close to the anatomical structure *in-vivo*.

The basic idea of this model is the treatment of blood flow through extra- and intracranial vessels as a hydraulic circuit. This is a standard way to describe blood flow dynamics as can be found in references [1–4]. The advantage of this approach is the portability of the fundamental laws of electric circuits to hydraulic circuits, like Ohm’s and Kirchhoff’s law.

*Corresponding author. Email: sdaun@mi.uni-koeln.de

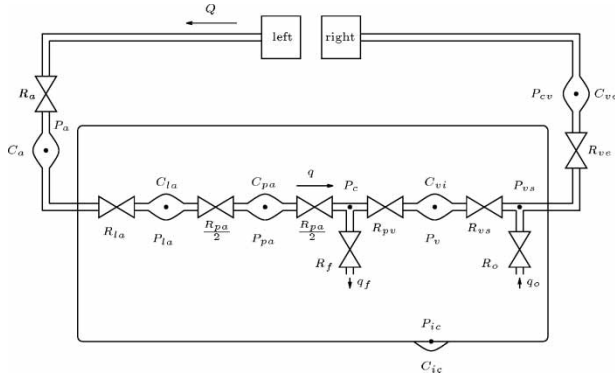


Figure 1. Biomechanical analog of the mathematical model, in which resistances are represented with restrictions and compliances with bulges. P_a , systemic arterial pressure; R_a and C_a , systemic arterial resistance and compliance; Q , cardiac output from the left heart, only a fraction of it goes into head; P_{ia} , R_{ia} and C_{ia} , pressure, resistance and compliance of large intracranial arteries, respectively; P_{pa} , R_{pa} and C_{pa} , pressure, resistance and compliance of pial arterioles, respectively; P_c , capillary pressure; q , tissue cerebral blood flow; R_{pv} , resistance of proximal cerebral veins; C_{vi} , intracranial venous compliance; P_v , cerebral venous pressure; P_{vs} and R_{vs} , sinus venous pressure and resistance of the terminal intracranial veins, respectively; q_f and q_o , cerebrospinal fluid flow into and out of the craniospinal space, respectively; R_f and R_o , inflow and outflow resistance; P_{ic} and C_{ic} , intracranial pressure and compliance, respectively; P_{cv} , central venous pressure, R_{ve} and C_{ve} , resistance and compliance of the extracranial veins.

The hydraulic circuit was extended by several physiological mechanisms. First work in this direction was done by Ursino *et al.* [1] by including the autoregulation and the CO_2 reactivity. In this work, the following additional features are treated to get a more realistic and physiologically applicable model (figure 1):

- the extracranial pathways which close the circulation of blood;
- the pulsatility of blood flow, which is given by using a periodic function for the cardiac output Q as input to the systemic circulation;
- the regulation mechanism, which describes the dependence of cerebral blood flow on the production of nitric oxide (NO) at the endothelial cells of the small cerebral arteries and arterioles (NO reactivity);
- the interaction between CO_2 and NO reactivity;
- the description of the release of catecholamines into the blood and its impact on heart frequency, cardiac output and thus blood pressure.

The paper is organized as follows: in section 2, a qualitative model description is given. The process of parameter estimation is described in section 3 and numerical simulations and validation results are shown in section 4. In the last section, the mathematical model is discussed and an outlook is given.

2. Qualitative model description

The model is qualitatively presented, with attention focused on its new aspects.

2.1 Extracranial arterial pathways

The work of Ursino *et al.* [2] is used as the basic model for the new investigations. There only the cerebral hemodynamics are considered and the blood pressure P_a is chosen as a constant input parameter for the cerebral blood circulation. In this work, the extracranial arterial pathways are also modelled and thus the arterial blood pressure is no constant parameter but depends on time t , cardiac output Q and thus on cardiac parameters.

The segment of the extracranial arteries from the left heart to the large cerebral arteries is, like the other segments of the model, described by the hydraulic resistance R_a and the hydraulic compliance C_a . The amount of blood ejected from the heart into the aorta in a certain time is modelled by a function Q , which will be described later. Because of the theory of hydraulic circuits, blood volume changes dV/dt in the extracranial and intracranial arteries and veins are given by the difference of blood flow into and out of these vessels. The compliances C are synonymous with the storage capacities of the arteries and veins. Therefore, the blood volume changes dV_a/dt are given by the difference of the blood flow into the aorta (Q) minus the systemic blood flow out of the aorta through all organs of the body $((P_a - P_{cv})/R_s)$:

$$\frac{dV_a}{dt} = C_a \frac{dP_a}{dt} = Q - \frac{P_a - P_{cv}}{R_s} \quad (1)$$

where Q is cardiac output, P_a arterial, P_{cv} central venous pressure and R_s systemic resistance. The blood flow through the vessels is calculated by Ohm's law. Since $P_{cv} \ll P_a$ changes in blood pressure dP_a/dt are approximately given by

$$\frac{dP_a}{dt} = \frac{1}{C_a} \left(Q - \frac{P_a}{R_s} \right). \quad (2)$$

The fraction of cardiac output Q which goes into head is then given by $(P_a - P_{ia})/R_{ia}$ and the value of the compliance C_a is corresponding to [5] $C_a = 0.0042$ ml/mm Hg.

2.2 Cardiac output

The model function for cardiac output Q , developed by Stevens *et al.* [6], is used to get a pulsatile blood flow throughout the circulatory system. The cardiac output Q is modelled by defining an interior function which oscillates with the frequency of the heart pulse and an envelope function for these interior oscillations. The product of these two functions is then normalized and the parameters are calibrated with physical rat data. The provisional flow function $Q_3(t, n, \Phi)$ is then given by

$$Q_3(t, n, \Phi) = Q_1(t, n) \cdot Q_2(t, \Phi), \quad (3)$$

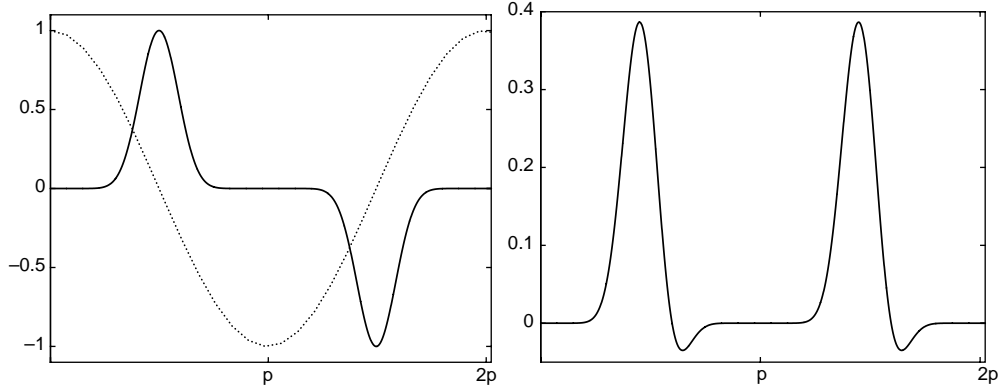


Figure 2. Left: The envelope function Q_1 (solid curve) and the interior function Q_2 (dashed curve) for $n = 13$ and $\Phi = 0$. Right: The flow function $Q_3(t, 13, \pi/10)$.

where the envelope function is defined by

$$Q_1(t, n) = \sin^n(\omega t) \text{ with } n \text{ odd} \quad (4)$$

and the interior function has the form

$$Q_2(t, \Phi) = \cos(\omega t - \Phi) \quad (5)$$

with ω one half of the basic frequency of the heart pulse and Φ a suitable phase angle. Generally Φ lies in the range $0 < \Phi \leq \pi/2$. If $\Phi = 0$, cardiac outflow will equal backflow. There is nearly zero backflow if $\Phi > \pi/6$. For $n = 13$ and $\Phi = 0$, these two functions are shown in figure 2.

The Q must be normalized and calibrated to produce a good model function for cardiac output. The set of calibration parameters for this model function includes the stroke volume ν , the heart rate b , and the phase angle Φ . To fit the experimental data given by reference [5], the parameters are chosen as follows:

the heart rate $b = 378/60$ beats per second, the mean value for cardiac output $\bar{Q} = \nu b = 70/60 \text{ ml s}^{-1}$ thus the stroke volume $\nu = \bar{Q}/b = 0.1852 \text{ ml per second}$ the phase angle $\Phi = \pi/10$.

Once appropriate values of these calibration parameters are chosen, it is possible to determine the period $p = 1/b$ of the cycle and the frequency $\omega = \pi/p$.

By normalizing the model function Q_3 so that the total outflow over one period equals ν one gets

$$\begin{aligned} Q(t, n, \Phi) &= \frac{\nu}{A(n, \Phi)} Q_3(t, n, \Phi) \\ &= \frac{\nu}{A(n, \Phi)} \sin^n(\omega t) \cos(\omega t - \Phi) \end{aligned} \quad (6)$$

where

$$\bar{A}(n, \Phi) = \int_0^p Q_3(t, n, \Phi) dt. \quad (7)$$

With the relation $\omega = \pi/p$ and noting that

$$\begin{aligned} \bar{A}(n, \Phi) &= \int_0^\pi \sin^n(t) \cos(t - \Phi) dt \\ &= \frac{\sqrt{\pi} \Gamma(1 + \frac{n}{2}) \sin(\Phi)}{\Gamma(\frac{3+n}{2})} \end{aligned} \quad (8)$$

with Γ the Euler gamma function, one gets

$$\begin{aligned} A(n, \Phi) &= \int_0^p Q_3(t, n, \Phi) dt \\ &= \int_0^\pi \sin^n(\omega t) \cos(\omega t - \Phi) dt = \frac{\bar{A}(n, \Phi)}{\omega}. \end{aligned} \quad (9)$$

An example for $Q(t, n, \Phi)$ is given in figure 3. The narrowness of the output function Q is determined by the choice of n . A large n represents a small systole period. Using a value of $n = 13$ results in a systole period approximately $1/3$ of the cardiac cycle, consistent with values given by many of the standard texts in physiology.

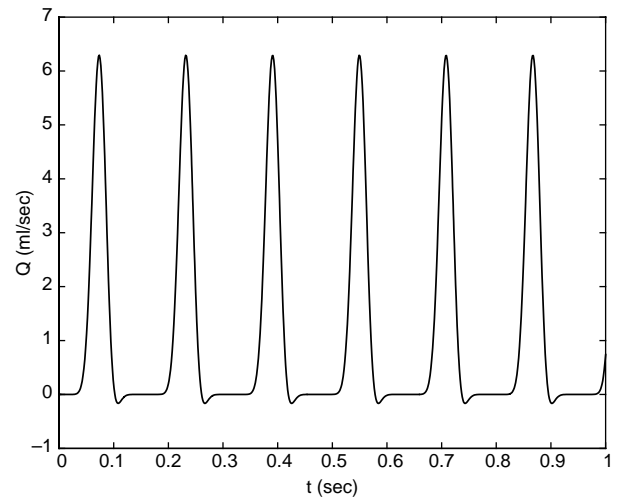


Figure 3. Cardiac output Q of rat is simulated by the model function with heart rate $b = 378/60$ beats per second, stroke volume $\nu = 0.1852 \text{ ml per beat}$, $n = 13$, and $\Phi = \pi/10$.

2.3 Intracranial hemodynamics

The Monro–Kellie doctrine implies that any volume variation in an intracranial compartment causes a compression or dislocation of the other volumes. These changes in the compartments are accompanied by an alteration in intracranial pressure P_{ic} . The intracranial compliance C_{ic} , which represents the capacity of the craniospinal system to store a volume load, is according to Ursino *et al.* [2] assumed to be inversely proportional to intracranial pressure through a constant parameter

$$C_{ic} = \frac{1}{k_E \cdot P_{ic}}. \quad (10)$$

In this model, volume changes in the craniospinal space are ascribed to four compartments: large and middle cerebral arteries dV_{la}/dt , pial arteries and arterioles dV_{pa}/dt , cerebral veins dV_v/dt , and the H_2O compartment dV_{H_2O}/dt . According to the Monro–Kellie doctrine the following conservation equation holds

$$C_{ic} \cdot \frac{dP_{ic}}{dt} = \frac{dV_{la}}{dt} + \frac{dV_{pa}}{dt} + \frac{dV_v}{dt} + \frac{dV_{H_2O}}{dt} \quad (11)$$

with time t . The biomechanical analog in figure 1 represents the four intracranial compartments considered in the model, together with the extracranial arterial and venous pathways.

2.4 Large and middle cerebral arteries

The first intracranial segment of the model represents the circulation of blood in the large and middle cerebral arteries. The hemodynamic is described by a hydraulic resistance R_{la} and a hydraulic compliance C_{la} . In contrast to the model of Ursino *et al.* [2] changes in the storage capacity C_{la} and thus on the blood volume V_{la} and the pressure P_{la} are modelled. The changes in volume in this segment dV_{la}/dt are given by

$$\frac{dV_{la}}{dt} = \frac{P_a - P_{la}}{R_{la}} - \frac{P_{la} - P_{pa}}{R_{pa}/2}, \quad (12)$$

where P_{pa} and R_{pa} are pressure and resistance of the pial arteries and arterioles, respectively.

Because the impact of the cerebrovascular regulation mechanisms on these intracranial arteries is very small, the resistance R_{la} is assumed to be constant. Further on, volume changes in this compartment depend only on changes in transmural pressure ($P_{la} - P_{ic}$) and not on changes in compliance C_{la} , since these vessels behave passively. Thus the following equation holds

$$\frac{dV_{la}}{dt} = C_{la} \left(\frac{dP_{la}}{dt} - \frac{dP_{ic}}{dt} \right). \quad (13)$$

With these two equations in mind one gets a differential equation which describes pressure changes dP_{la}/dt in the

large and middle cerebral arteries:

$$\frac{dP_{la}}{dt} = \frac{1}{C_{la}} \left(\frac{P_a - P_{la}}{R_{la}} - \frac{P_{la} - P_{pa}}{R_{pa}/2} \right) + \frac{dP_{ic}}{dt}. \quad (14)$$

The compliance of these vessels is assumed to be inversely proportional to the transmural pressure

$$C_{la} = \frac{k_{C_{la}}}{P_{la} - P_{ic}} \quad (15)$$

with $k_{C_{la}}$ the proportionality constant.

2.5 Pial arteries and arterioles

In this compartment of the model all sections of the cerebrovascular bed directly under the control of the regulatory mechanisms are comprised. This pial arterial segment is described by a hydraulic resistance R_{pa} and a hydraulic compliance C_{pa} . Both of these parameters are regulated by cerebrovascular control mechanisms. The two equations which describe the changes in volume dV_{pa}/dt in this segment and the calculation of the pressure at the cerebral capillaries P_c (applying Kirchhoff's law) are given in reference [2].

With these three equations the pressure change dP_{pa}/dt in the pial arterial compartment is described by

$$\begin{aligned} \frac{dP_{pa}}{dt} = \frac{1}{C_{pa}} \left[\frac{P_{la} - P_{pa}}{R_{pa}/2} - \frac{P_{pa} - P_c}{R_{pa}/2} - \frac{dC_{pa}}{dt} (P_{pa} - P_{ic}) \right] \\ + \frac{dP_{ic}}{dt}. \end{aligned} \quad (16)$$

2.6 Intracranial and extracranial venous circulation

The intracranial vascular bed of the veins is described by a series arrangement of two segments. The first, from the small postcapillary venules to the large cerebral veins, contains the resistance R_{pv} and the venous compliance C_{vi} . Corresponding to reference [2], the compliance is calculated by

$$C_{vi} = \frac{k_{ven}}{P_v - P_{ic} - P_{v1}}, \quad (17)$$

where k_{ven} is a constant parameter and P_{v1} represents the transmural pressure value at which cerebral veins collapse.

Using the equations defined in reference [2], which describe the volume changes dV_v/dt of this venous compartment, the pressure changes dP_v/dt are given by

$$\frac{dP_v}{dt} = \frac{1}{C_{vi}} \left(\frac{P_c - P_v}{R_{pv}} - \frac{P_v - P_{vs}}{R_{vs}} \right) + \frac{dP_{ic}}{dt}, \quad (18)$$

where R_{vs} is the resistance of the terminal intracranial veins and P_{vs} the pressure at the dural sinuses.

The second segment represents the terminal intracranial veins (e.g. lateral lakes). During intracranial hypertension

these vessels collide or narrow at their entrance into the dural sinuses, with a mechanism similar to that of a starling resistor (cf. [2]). Because of this phenomenon the resistance R_{vs} depends on the pressures of the system in the following way:

$$R_{vs} = \frac{P_v - P_{vs}}{P_v - P_{ic}} \cdot R_{vs1}, \quad (19)$$

where R_{vs1} represents the terminal vein resistance when $P_{ic} = P_{vs}$.

In contrast to the model of Ursino *et al.* [2] the sinus venous pressure P_{vs} is not assumed to be constant, but depends on time and the other pressures of the system and is calculated by Kirchhoff's law

$$\frac{P_v - P_{vs}}{R_{vs}} + q_o = \frac{P_{vs} - P_{cv}}{R_{ve}}. \quad (20)$$

Since the water backflow at the dural sinuses q_o is negligible in comparison to the blood flows, it is assumed to be zero.

The extracranial venous circulation from the dural sinuses through the vena cava back to the heart is described by the hydraulic resistance R_{ve} and the hydraulic compliance C_{ve} . Because no mechanisms acting on these blood vessels are taken into account, these parameters are assumed to be constant.

2.7 H₂O compartment

Under clinical aspects the formation of cerebral edema after head injury has to be described by the model. This mechanism is reproduced by water outflow at the capillaries into the craniospinal space and water backflow at the dural sinuses. It is assumed that the two processes are passive and unidirectional, thus the following equations hold:

$$q_f = \begin{cases} \frac{P_c - P_{ic}}{R_f} & \text{if } P_c > P_{ic} \\ 0 & \text{else} \end{cases} \quad (21)$$

$$q_o = \begin{cases} \frac{P_{ic} - P_{vs}}{R_o} & \text{if } P_{ic} > P_{vs} \\ 0 & \text{else.} \end{cases} \quad (22)$$

The case of a severe cerebral edema is simulated by decreasing the outflow resistance R_f , thus increasing the outflow q_f , whereas the backflow q_o is assumed to be constant and small all the time. Under physiological conditions q_f and q_o are approximately zero. Changes in volume in this H₂O compartment are given by $dV_{H_2O}/dt = q_f - q_o$.

2.8 Cerebrovascular regulation mechanisms

Cerebrovascular regulation mechanisms work by modifying the resistance R_{pa} and the compliance C_{pa} (and hence

the blood volume) in the pial arterial–arteriolar vasculature.

In this section, three mechanisms are considered which regulate cerebral blood flow. The effects of two of them, like autoregulation and CO₂ reactivity, are described in [2]. One new cerebrovascular regulation mechanism, the NO reactivity, is inserted into the model and its effect on the pial arterial compliance is modelled by using the given idea of a sigmoidal relationship of the whole regulation process.

2.8.1 Autoregulation. The cerebral autoregulation describes the ability of certain vessels to keep the cerebral blood flow (CBF) relatively constant despite changes in perfusion pressure.

As you can see in the upper branch of figure 4, it is assumed that autoregulation is activated by changes in CBF. The impact of this mechanism on the pial arterial vessels is described by a first-order low-pass filter dynamic with time constant τ_{aut} and gain G_{aut} (cf. [2])

$$\tau_{aut} \frac{dx_{aut}}{dt} = -x_{aut} + G_{aut} \left(\frac{q - q_n}{q_n} \right), \quad (23)$$

where q is the measured CBF and q_n the cerebral blood flow under basal conditions.

The cerebral blood flow q can be calculated by Ohm's law

$$q = \frac{P_{pa} - P_c}{R_{pa}/2}. \quad (24)$$

With this relation, we get a basal value for blood flow through the pial arteries of $q_n = 0.1696 \text{ ml s}^{-1}$. The value of the gain G_{aut} is given by fitting the autoregulation curve of [7].

2.8.2 CO₂ reactivity. The CO₂ reactivity describes the dependence of cerebral blood flow on arterial CO₂ pressure P_{aCO_2} .

The branch in the middle of figure 4 represents the CO₂ reactivity, which is activated by changes in P_{aCO_2} and described by a first-order low-pass filter dynamic with time constant τ_{CO_2} and gain G_{CO_2} (cf. [2])

$$\tau_{CO_2} \frac{dx_{CO_2}}{dt} = -x_{CO_2} + G_{CO_2} A_{CO_2} \log_{10} \left(\frac{P_{aCO_2}}{P_{aCO_2n}} \right), \quad (25)$$

where P_{aCO_2n} is the CO₂ pressure under basal conditions, corresponding to [8] it is $P_{aCO_2n} = 33 \text{ mm Hg}$. A_{CO_2} is a corrective factor, which will be described later. The value of the gain G_{CO_2} is obtained by fitting the data of Iadecola *et al.* [9].

2.8.3 NO reactivity. The NO reactivity describes the dependence of cerebral blood flow on the production rate of NO at the endothelial cells of the pial vessels q_{NO} .

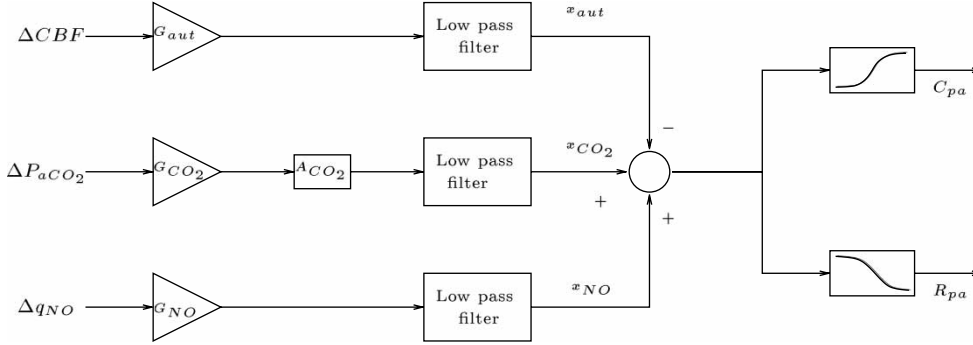


Figure 4. Block diagram describing the action of cerebrovascular regulation mechanisms according to the present model. The upper branch describes autoregulation, the middle branch indicates CO₂ response, and the lower branch describes NO reactivity. The input quantity for autoregulation is cerebral blood flow change ($\Delta CBF = \frac{q - q_n}{q_n}$). The input quantities for the CO₂ and NO mechanisms are the logarithm of arterial CO₂ tension (P_{aCO_2}), i.e. $\Delta P_{aCO_2} = \log_{10}(P_{aCO_2}/P_{aCO_2n})$, and the logarithm of NO production (q_{NO}), i.e. $\Delta q_{NO} = \log_{10}(q_{NO}/q_{NO_n})$, respectively. The dynamics of these mechanisms are simulated by means of a gain factor (G) and a first-order low-pass filter with time constant τ . The variables x_{aut} , x_{CO_2} and x_{NO} are three state variables of the model that account for the effect of autoregulation, CO₂ reactivity and NO reactivity, respectively, they are given in ml/mm Hg, q_n , P_{aCO_2n} and q_{NO_n} are set points for the regulatory mechanisms. The gain factor of the CO₂ reactivity is multiplied by a corrective factor A_{CO_2} , because as a consequence of tissue ischemia CO₂ reactivity is depressed at low CBF levels. These three mechanisms interact nonlinearly through a sigmoidal static relationship, and therefore producing changes in pial arterial compliance and resistance.

For this regulation mechanism the following assumptions are made: first, only the impact of nitric oxide (NO) on the smooth muscle cells of pial vessels is considered, whereas the response of large arteries and veins on nitric oxide is neglected. Second, although there are distinct sources of NO in brain, e.g. neuronal or endothelial NO, the model does not differentiate the different sources of NO. Furthermore, no interactions of NO with other substances are considered.

In the case of a head injury production of nitric oxide occurs at the endothelial cells of the pial arteries and arterioles. These NO molecules migrate through the vessel wall to the smooth muscle cells and activate a substance called guanylcyclase there, which causes a higher production of guanosine 3',5'-cyclic monophosphate (cGMP) with subsequent relaxation. In contrast any decrease in NO production causes constriction of the pial vessels.

The lower branch of figure 4 represents the NO reactivity, which is activated by changes in the NO production rate q_{NO} and described by a first-order low-pass filter dynamic with time constant τ_{NO} and gain G_{NO}

$$\tau_{NO} \frac{dx_{NO}}{dt} = -x_{NO} + G_{NO} \log_{10} \left(\frac{q_{NO}}{q_{NO_n}} \right), \quad (26)$$

where q_{NO_n} defines the NO production rate under basal conditions, corresponding to [10] it is $q_{NO_n} = 54.1$ ng/g tissue.

It is assumed that the production rate q_{NO} is linearly correlated with the concentration of nitric oxide C_{NO} in the vessel wall and that the vessel radius dependence on \log_{10} of NO concentration is almost linear in the range of physiological conditions (cf. [11,12]). These are the reasons why the logarithm of q_{NO} is chosen as input to the controller. The regulation gain G_{NO} is then given by fitting the data of Wang *et al.* [13].

The time constants of these three regulation mechanisms τ_{aut} , τ_{CO_2} and τ_{NO} are approximated by using data of references [9,13,14], the values are 20, 50 and 40 s, respectively.

The minus sign at the upper branch of figure 4 means that an increase in cerebral blood flow causes vasoconstriction, with a decrease in pial compliance and an increase in pial resistance as consequence. Whereas, the plus signs at the middle and lower branches of figure 4, mean that an increase in arterial CO₂ pressure or in endothelial NO production causes vasodilation, with an increase in pial compliance and a decrease in pial resistance as consequence.

2.9 Impact of the regulation mechanisms on C_{pa} and R_{pa} and their interactions

According to [15], the impact of NO production at the endothelial cells on arterial CO₂ pressure is very small. Therefore, only the effect of P_{aCO_2} on the production rate q_{NO} is considered in this model. According to [16], an 70% increase in arterial CO₂ pressure yields an 20% increase in the NO production rate. It is assumed that these two mechanisms are connected linearly by the following equation

$$q_{NO} = 0.4332 P_{aCO_2} + 39.8048. \quad (27)$$

Autoregulation is influenced by NO reactivity because of changes in CBF. The model considers this effect although these two mechanisms are not directly connected.

The three regulation mechanisms described above do not act linearly on the pial vessels. The first nonlinearity is given by the fact that the strength of CO₂ reactivity is not independent of CBF level but decreases significantly during severe ischemia. Such a severe ischemia is associated with tissue acidosis, which buffers the effect

of CO_2 changes on perivascular pH. This phenomenon is modelled by the corrective factor A_{CO_2}

$$A_{\text{CO}_2} = \frac{1}{1 + \exp \{[-k_{\text{CO}_2}(q - q_n)/q_n] - b_{\text{CO}_2}\}} \quad (28)$$

with constant parameters k_{CO_2} and b_{CO_2} (cf. [2]).

Another nonlinearity is given by the fact that the whole regulation process is not just the sum of these three mechanisms but is described by a sigmoidal relationship with upper and lower saturation levels. Adapting the situation of Ursino *et al.* [2] to three regulation mechanisms one gets

$$C_{\text{pa}} = \frac{(C_{\text{pan}} - \Delta C_{\text{pa}}/2) + (C_{\text{pan}} + \Delta C_{\text{pa}}/2) \cdot \exp[(x_{\text{CO}_2} + x_{\text{NO}} - x_{\text{aut}})/k_{C_{\text{pa}}}]}{1 + \exp[(x_{\text{CO}_2} + x_{\text{NO}} - x_{\text{aut}})/k_{C_{\text{pa}}}]}$$
 (29)

where C_{pan} is the pial arterial compliance under basal conditions, ΔC_{pa} the change in compliance and $k_{C_{\text{pa}}}$ a constant parameter.

This equation shows that any decrease in CBF, any increase in arterial CO_2 pressure and any increase in the NO production rate causes vasodilation with an increase in pial arterial compliance C_{pa} . On the other hand, any increase in CBF, any decrease in arterial CO_2 pressure and any decrease in NO production rate causes vasoconstriction with a reduction in compliance C_{pa} .

A value for the constant parameter $k_{C_{\text{pa}}}$ was given to set the central slope of the sigmoidal curve to +1. This condition is obtained by assuming $k_{C_{\text{pa}}} = \Delta C_{\text{pa}}/4$.

An important point is that this sigmoidal curve is not symmetrical: the increase in blood volume caused by vasodilation is greater than the decrease of blood volume caused by vasoconstriction. That is the reason why two different values of the parameter ΔC_{pa} have to be chosen depending on whether vasodilation or vasoconstriction is considered. It is

$$\begin{cases} x_{\text{CO}_2} + x_{\text{NO}} - x_{\text{aut}} > 0: & \Delta C_{\text{pa}} = \Delta C_{\text{pa}1}; k_{C_{\text{pa}}} = \Delta C_{\text{pa}1}/4 \\ x_{\text{CO}_2} + x_{\text{NO}} - x_{\text{aut}} < 0: & \Delta C_{\text{pa}} = \Delta C_{\text{pa}2}; k_{C_{\text{pa}}} = \Delta C_{\text{pa}2}/4. \end{cases} \quad (30)$$

Consider equation (29): For $(x_{\text{CO}_2} + x_{\text{NO}} - x_{\text{aut}}) \rightarrow \infty$ one gets $C_{\text{pa}} \rightarrow (C_{\text{pan}} + \Delta C_{\text{pa}1}/2)$ and $(x_{\text{CO}_2} + x_{\text{NO}} - x_{\text{aut}}) \rightarrow -\infty$ yields $C_{\text{pa}} \rightarrow (C_{\text{pan}} - \Delta C_{\text{pa}2}/2)$. That means $(C_{\text{pan}} + \Delta C_{\text{pa}1}/2)$ and $(C_{\text{pan}} - \Delta C_{\text{pa}2}/2)$ are the upper and lower saturation levels of the sigmoidal curve, respectively.

An expression for dC_{pa}/dt is obtained by differentiating equation (29) to

$$\begin{aligned} \frac{dC_{\text{pa}}}{dt} &= \frac{\Delta C_{\text{pa}}}{k_{C_{\text{pa}}}} \cdot \frac{\exp[(x_{\text{CO}_2} + x_{\text{NO}} - x_{\text{aut}})/k_{C_{\text{pa}}}]}{\{1 + \exp[(x_{\text{CO}_2} + x_{\text{NO}} - x_{\text{aut}})/k_{C_{\text{pa}}}]\}^2} \\ &\times \frac{d(x_{\text{CO}_2} + x_{\text{NO}} - x_{\text{aut}})}{dt}. \end{aligned} \quad (31)$$

The cerebrovascular control mechanisms act also on the hydraulic pial arterial resistance R_{pa} . Because the blood volume is directly proportional to the inner radius second power, while the resistance is inversely proportional to inner radius fourth power, the following relationship holds between the pial arterial volume and resistance (cf. [2])

$$R_{\text{pa}} = \frac{k_{\text{R}} C_{\text{pan}}^2}{V_{\text{pa}}^2} \quad (32)$$

where k_{R} is a constant parameter.

2.10 Norepinephrine and its impact on heart rate

Norepinephrine is the principal mediator of the sympathetic nervous system. Cardiac function is modulated in many aspects by norepinephrine. The primary effect of this substance is an increase in heart rate and thus an increase in cardiac output Q (figure 5).

The changes of the norepinephrine concentration in blood $d[\text{NE}]/dt$ are described by the equation

$$\frac{d[\text{NE}]}{dt} = r - \alpha_{\text{NE}}[\text{NE}], \quad (33)$$

where r is the constant NE release during sympathetic nerve stimulation and α_{NE} is the elimination rate.

Because absolute values of $[\text{NE}]$ are unknown r can be fixed to one in the case of sympathetic nerve activation without loss of generality, otherwise r is chosen as zero. That means this mechanism of NE release is switched on and off by the parameter r and the parameter α_{NE} specifies the strength of sympathetic nerve stimulation and can be varied throughout the simulations.

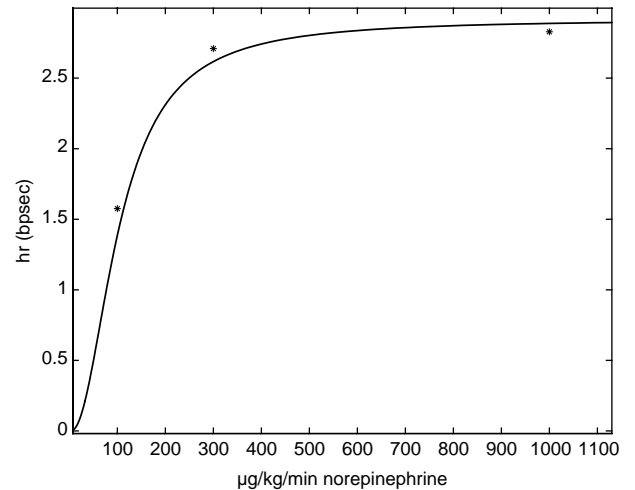


Figure 5. Dependence of heart rate variation hr on the amount of norepinephrine in blood. Model results (solid curve) and measured data of Muchitsch *et al.* ([17]).

The heart rate response to a steplike increase of the norepinephrine concentration [NE] is described by a first-order low-pass filter dynamic with time constant τ_{hr}

$$\tau_{hr} \frac{dhr}{dt} = -hr + G([NE]), \quad (34)$$

where hr is the heart rate variation. The steady-state heart rate response $G([NE])$ is, according to [18], defined by

$$\Delta HR = G([NE]) = \frac{\Delta HR_{\max} [NE]^2}{K_{NE}^2 + [NE]^2}, \quad (35)$$

where K_{NE} is the NE concentration producing a half maximum response and ΔHR_{\max} is the maximum value of ΔHR . Corresponding to Muchitsch *et al.* [17], the values of these parameters are 175 bpm and $100 \mu\text{g kg}^{-1} \text{min}$, respectively and the time constant τ_{hr} is 5 s.

The new heart rate \bar{b} is then given by adding the heart rate variation hr to b

$$\bar{b} = b + hr.$$

3. Parameter estimation

The estimation of systemic parameters under basal conditions is described now. The values of the compliances in the craniospinal space, like C_{la} , C_{pa} and C_{vi} , and the intracranial compliance C_{ic} were fitted by using pressure curves of these compartments. The values were fitted in the way that the model amplitudes of the pressures in each compartment are equal to the given physiological amplitudes of pressures (cf. [19–22]).

The basal value of the resistance of the large intracranial arteries is calculated by using the Hagen–Poiseuille law $R = (8\eta l)/(r^4 \pi)$. All other model resistances, R_s , R_{pa} , R_{pv} , R_{vs} and R_{ve} are calculated by using the mean pressure values in each compartment (see [19–21]) and solving the differential equations defined above. All model parameters under basal conditions are given in table 1.

Table 1. Basal values of model parameters.

$C_a = 0.0042 \text{ ml/mm Hg}$	$R_s = 99.4286 \text{ mm Hg} \cdot \text{s} \cdot \text{ml}^{-1}$
$n = 13$	$B = 378/60 \text{ beats per second}$
$v = 0.1852 \text{ ml per beat}$	$k_{C_{la}} = 0.0305 \text{ ml}$
$R_{la} = 47.1609 \text{ mm Hg} \cdot \text{s} \cdot \text{ml}^{-1}$	$k_R = 1.6258e + 06 \text{ mm Hg}^3 \cdot \text{s} \cdot \text{ml}^{-1}$
$C_{pan} = 4.7277e - 07 \text{ ml/mm Hg}$	$\Delta C_{pa1} = 6.6188e - 06 \text{ ml/mm Hg}$
$\Delta C_{pa2} = 3.7822e - 07 \text{ ml/mm Hg}$	$R_{pv} = 29.4756 \text{ mm Hg} \cdot \text{s} \cdot \text{ml}^{-1}$
$R_f = 2830 \text{ mm Hg} \cdot \text{s} \cdot \text{ml}^{-1}$	$R_o = 1783 \text{ mm Hg} \cdot \text{s} \cdot \text{ml}^{-1}$
$q_n = 0.1696 \text{ ml} \cdot \text{s}^{-1}$	$\tau_{aut} = 20 \text{ s}$
$G_{aut} = 0.00006$	$\tau_{CO_2} = 50 \text{ s}$
$G_{CO_2} = 0.000435$	$P_{aCO_2n} = 33 \text{ mm Hg}$
$\tau_{NO} = 40 \text{ s}$	$G_{NO} = 0.000125$
$q_{NO_n} = 54.1 \text{ ng/g tissue}$	$k_{CO_2} = 27$
$b_{CO_2} = 19$	$k_{ven} = 4.9353e - 08 \text{ ml}$
$P_{cv} = 1.7 \text{ mm Hg}$	$R_{vs1} = 5.566 \text{ mm Hg} \cdot \text{s} \cdot \text{ml}^{-1}$
$P_{v1} = -2.5 \text{ mm Hg}$	$R_{ve} = 2.9476 \text{ mm Hg} \cdot \text{s} \cdot \text{ml}^{-1}$
$k_E = 41 \text{ ml}^{-1}$	$D_{\max} = 175/60 \text{ beats per second}$
$\tau_{hr} = 5 \text{ s}$	$k_{NE} = 100 \mu\text{g} \cdot \text{kg}^{-1} \cdot \text{min}$

4. Numerical simulations

With the parameters given in table 1 numerical simulations were performed to show that the model gives a reasonable and realistic description of the physiological system.

Figure 6 shows the simulated pressure in the aorta P_a and the intracranial pressure P_{ic} . These pressures agree with experimental data of Baumbach [20], who measured a systolic blood pressure of $134 \pm 7 \text{ mm Hg}$ and a diastolic pressure of $98 \pm 6 \text{ mm Hg}$ and with data of Holtzer *et al.* [22] who measured a mean intracranial pressure of $6 \pm 3 \text{ mm Hg}$ and an amplitude of the pressure curve of approximately 1.4 mm Hg .

The simulated pressure of the small arteries and arterioles in the left of figure 7 agrees with the measured data of $67 \pm 4 \text{ mm Hg}$ for the pial systolic pressure and $53 \pm 3 \text{ mm Hg}$ for the pial diastolic pressure by Baumbach [20]. Further on, the works of Gotoh *et al.* [19] and Sugiyama *et al.* [21] suggest a mean large cerebral arteries pressure of 108 mm Hg and an amplitude of 23 mm Hg , which agrees also with the simulated pressure curve in the right hand side part of the figure.

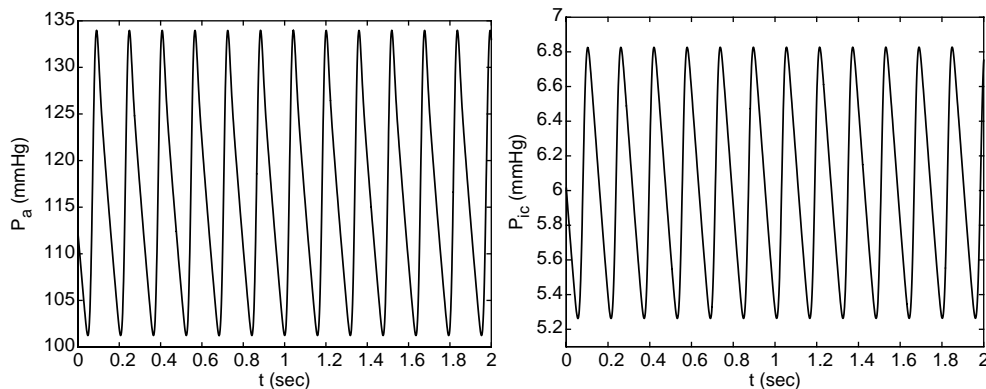


Figure 6. Left: simulated blood pressure in the aorta, received by solving equation (2). Right: simulated intracranial pressure curve, received by solving equation (11).

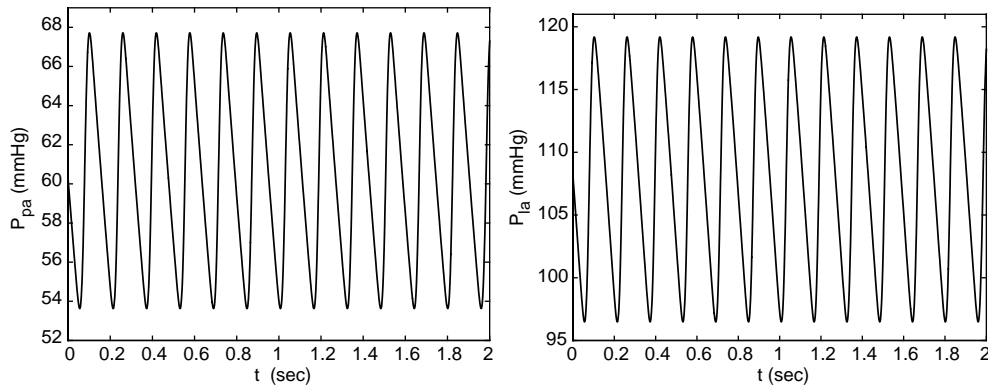


Figure 7. Left: simulated pressure curve of the pial arteries, received by solving equation (16). Right: simulated pressure curve of the large arteries, received by solving equation (14).

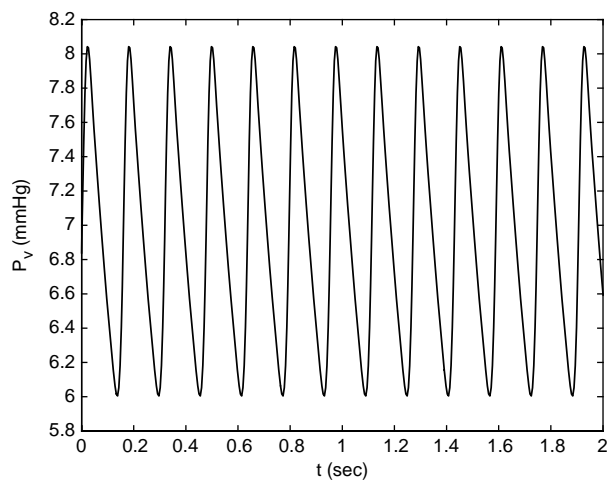


Figure 8. Simulated pressure curve of the cerebral veins, received by solving equation (18).

Figure 8 shows the simulated pressure of the cerebral veins P_v . A mean cerebral venous pressure of 7 ± 1 mm Hg is given by Mayhan and Heistad [23].

The simulated dependence of cerebral blood flow on arterial CO_2 pressure is shown in the left hand side part

of the figure 9. One observes a 230% increase in cerebral blood flow, if $P_{a\text{CO}_2}$ is changed from 34.3 to 49.2 mm Hg. This result corresponds to the measured data of Iadecola *et al.* [9]. Further on, the impact of NO on CBF is simulated and the result is given in the right of figure 9.

To show that the interaction between CO_2 and NO reactivity is modelled realistically, the dependence of $P_{a\text{CO}_2}$ on NO is simulated by calculating the CO_2 reactivity with the basal value of q_{NO} and with inhibition of NO production. The results are shown in figure 10: the solid curve is equal to the left curve in figure 9, since $q_{\text{NO}} = q_{\text{NO}n}$ and the dashed curve is the simulation result with inhibited NO production, $q_{\text{NO}} = 0.1 \cdot q_{\text{NO}n}$. The resulting decrease in CBF corresponds to the data of Wang *et al.* [13].

In addition to the numerical simulations described above, the impact of the sympathetic system, i.e. norepinephrine on heart rate and cardiac output, is simulated. The strength of sympathetic nerve stimulation is regulated by the parameter α_{NE} . Choosing a value of $\alpha_{\text{NE}} = 0.04$ corresponds to a stimulation with a frequency of 2 Hz and yields a release of norepinephrine like the one measured by Mokrane *et al.* [18]. Figure 11 shows the simulated increase of [NE] and the corresponding simulated hr response. Any increase in heart rate yields

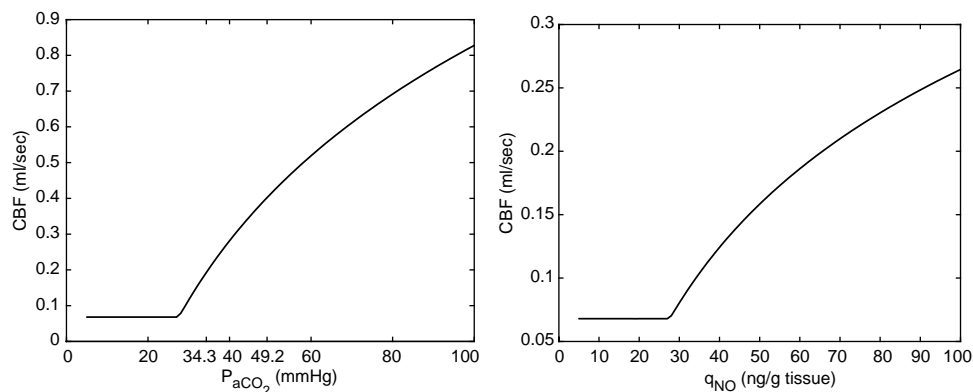


Figure 9. Left: dependence of CBF on arterial CO_2 pressure simulated by the model. Iadecola *et al.* [9] measured, by increasing $P_{a\text{CO}_2}$ from 34.3 to 49.2 mm Hg, an increase in cerebral blood flow of 230%. Right: the effect of changes in the NO production rate q_{NO} on cerebral blood flow is simulated by the model. The basal value of CBF ($q_n = 0.1696 \text{ ml s}^{-1}$) is given by a production rate of $q_{\text{NO}} = 54.1 \text{ ng/g tissue}$.

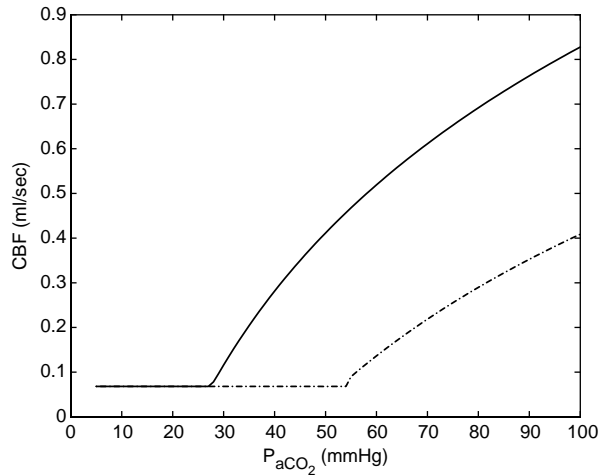


Figure 10. The dependence of CO_2 reactivity on NO is simulated by the model. The solid curve shows the dependence of CBF on $P_{a\text{CO}_2}$, here the linear relationship between NO production and CO_2 pressure (equation (27)) was used (see, figure 9). The dashed curve is the result of a model simulation with inhibition of NO production, $q_{\text{NO}} = 0.1q_{\text{NO}}$ (corresponding to Wang *et al.* [13]).

an increase in cardiac output Q (see equation (6)) and thus an increase in blood pressure P_a (see equation (2)). The impact of changes in heart rate on these cardiac parameters are simulated and the results are shown in figure 12. The mean value of cardiac output Q is used for simulations to show the increase in this variable and in blood pressure P_a more clearly.

5. Validation

For the validation of the model, experimental data of [24–29] were used as reference examples and compared to numerical simulations. These experimental results reflect special physiological situations and were not used to calibrate the model parameters.

The numerically simulated CO_2 reactivities for different values of mean arterial blood pressure and intracranial pressure are shown in figure 13. The top left of figure 13

shows the dependence of CBF under intracranial normotension ($P_{\text{ic}} = 4$ mm Hg) and different values of MAP: $A_1—P_a = 97$ mm Hg, $A_2—P_a = 77$ mm Hg, and $A_3—P_a = 64$ mm Hg. Decreasing the mean arterial blood pressure provides a decreased CBF for increased values of $P_{a\text{CO}_2}$. Hauerberg *et al.* [24] measured the dependence of cerebral blood flow on $P_{a\text{CO}_2}$ for the above given intracranial and blood pressure values. They also got a qualitative decreased CBF for decreased arterial and increased CO_2 pressure values.

The top right of figure 13 shows the dependence of cerebral blood flow on arterial CO_2 pressure under intracranial hypertension ($P_{\text{ic}} = 31$ mm Hg) and $B_1—P_a = 104$ mm Hg, $B_2—P_a = 123$ mm Hg. Increasing the mean arterial blood pressure yields an increase in CBF for higher values of $P_{a\text{CO}_2}$. This change in CBF was also measured by Hauerberg *et al.* [24] and they stated that the groups A_1 and B_2 are similar.

The bottom of figure 13 shows the CO_2 reactivity for a further increased intracranial pressure of 50 mm Hg and for $C_1—P_a = 104$ mm Hg and $C_2—P_a = 123$ mm Hg. Increasing the mean arterial blood pressure yields an increase in CBF for higher values of $P_{a\text{CO}_2}$ as can be seen in Hauerberg *et al.* [24], who also stated the similarity of the groups A_2 , B_1 and C_2 .

In figure 14 a simulated autoregulation curve is shown. For validation of the lower autoregulation limit, which lies in the range of 40 and 55 mm Hg, a work of Waschke *et al.* [25] is used. Corresponding to their experimental studies the mean arterial blood pressure is decreased from 116 to 86, 70, 55 and 40 mm Hg and the mean cerebral blood flow is calculated for the given pressure values by the model. In figure 15 the experimental results of Waschke *et al.* [25] are shown and compared with the simulated data. A significant decrease in cerebral blood flow, if blood pressure is decreased from 55 to 40 mm Hg, can be seen in the measured data as well as in the simulated data.

For validation of the upper autoregulation limit, which lies in the range of 150 and 160 mm Hg, a work of Schaller *et al.* [26] is used. The data of their control group of the

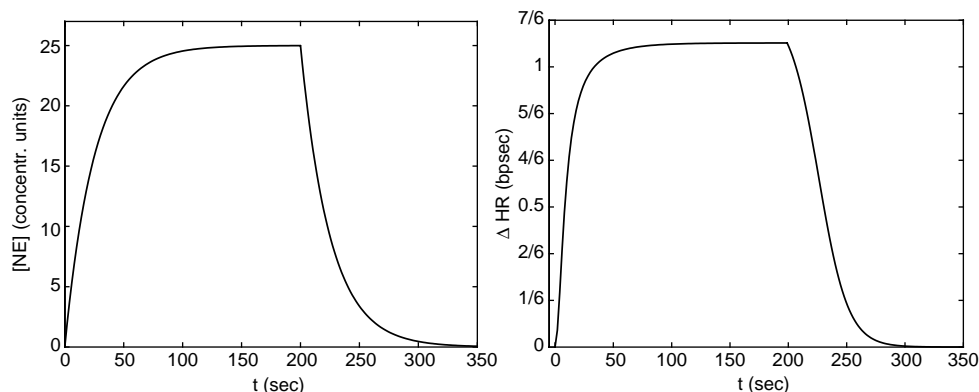


Figure 11. Left: simulated increase of [NE] with a stimulation domain of 0–200 s. Right: simulated heart rate response corresponding to these changes in [NE].

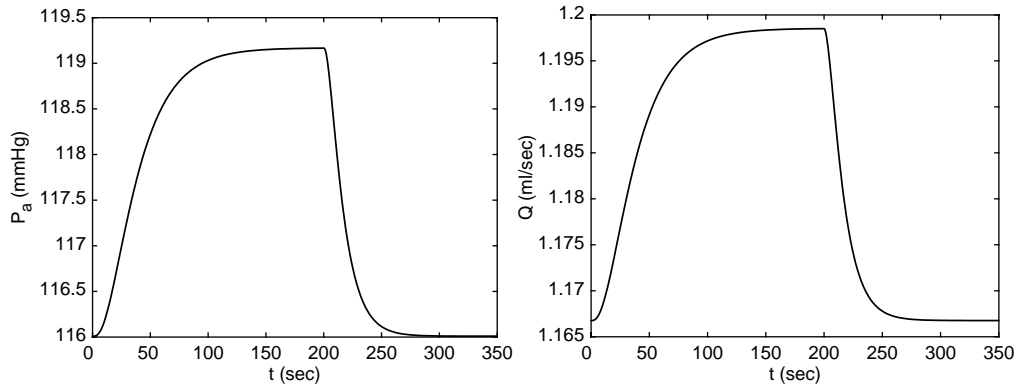


Figure 12. Left: simulated increase in blood pressure P_a . Right: simulated cardiac output response, to a stimulation interval of 0–200 s and with a stimulation intensity of $\alpha_{NE} = 0.04$.

investigated Wistar rats is compared with simulation results in figure 16, where mean arterial pressure is increased up to 10, 20, 30, 40 and 50 percent of its basal value and the corresponding cerebral blood flow is measured and calculated, respectively. One can see the increase in cerebral blood flow if blood pressure is increased up to 40–50% of its basal value in the measured data as well as in the simulated data.

Elevated intracranial pressure, the most serious acute sequela of traumatic brain injury, has direct impact on the lower autoregulation limit. Corresponding to the measured data of Engelborghs *et al.* [27] the intracranial pressure P_{ic} was changed from 6 to 33 mm Hg in the first 5 min after head injury. After another 23 h 55 min P_{ic} was decreased to 28 mm Hg. The changes in arterial CO_2 pressure and in heart rate b in the first day after brain damage, were

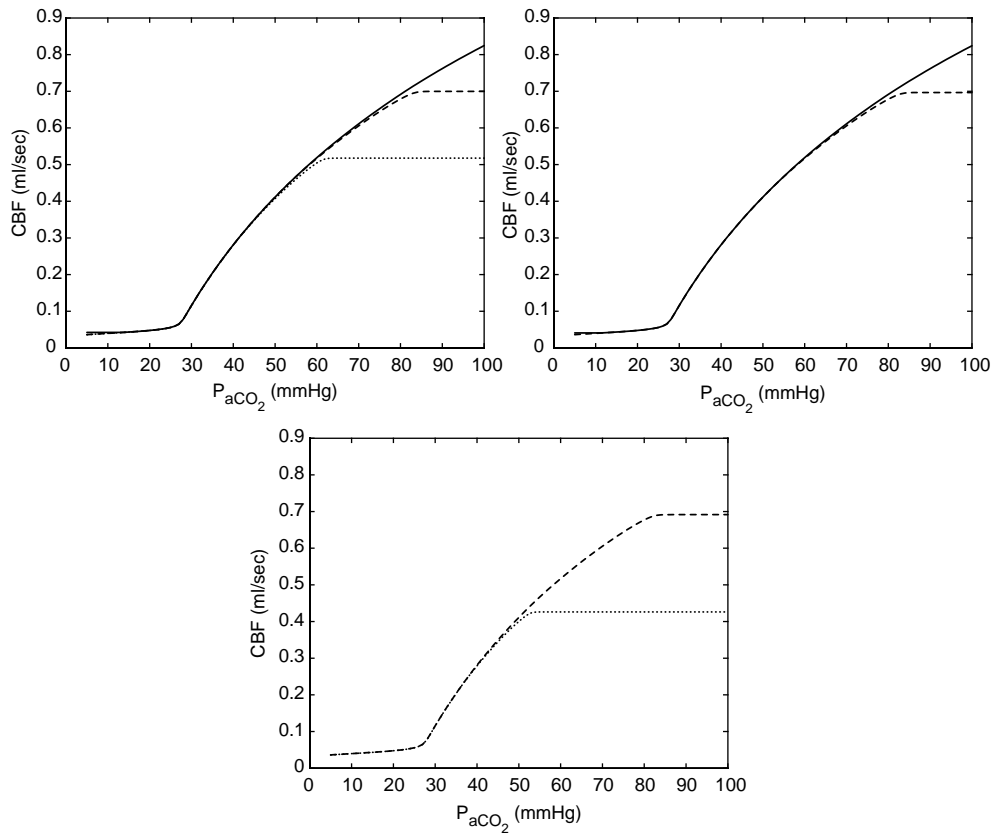


Figure 13. Top left: simulated dependence of CBF on P_{aCO_2} for $P_{ic} = 4$ mm Hg and $A_1 - P_a = 97$ mm Hg, solid line, $A_2 - P_a = 77$ mm Hg, dashed line and $A_3 - P_a = 64$ mm Hg, dotted line. Decreasing MAP under intracranial normotension results in a decrease in CBF for increased values of P_{aCO_2} (cf. [24]). Top right: simulated dependence of CBF on P_{aCO_2} for $P_{ic} = 31$ mm Hg and $B_1 - P_a = 104$ mm Hg, dashed line, $B_2 - P_a = 123$ mm Hg, solid line. Increasing MAP yields an increase in CBF for higher values of P_{aCO_2} . The simulation results of B_2 and A_1 are similar. These phenomena were also measured by Hauerberg *et al.* [24]. Bottom: simulated CO_2 reactivity for $P_{ic} = 50$ mm Hg and $C_1 - P_a = 104$ mm Hg, dotted line, and $C_2: P_a = 123$ mm Hg, dashed line. Increasing MAP yields an increase in CBF for higher values of P_{aCO_2} . The simulation results of C_2, A_2 and B_1 are similar. These phenomena were also measured by Hauerberg *et al.* [24].

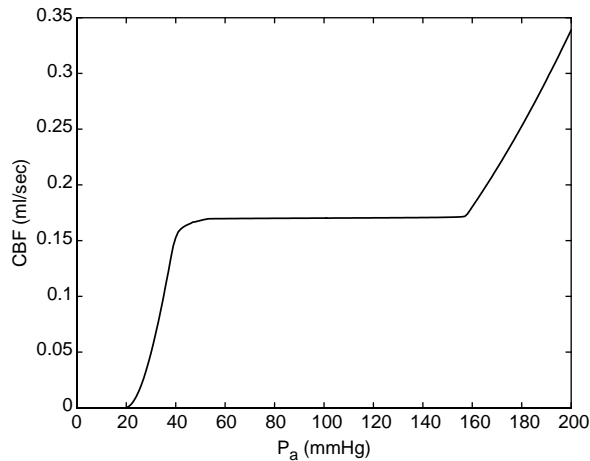


Figure 14. Autoregulation curve simulated by the model. The lower autoregulation limit lies, corresponding to Waschke *et al.* [25], in the range of 40 and 55 mmHg, the upper regulation limit was not investigated in their work. Corresponding to Schaller *et al.* [26] loss of autoregulation with increase in CBF occurred at approximately $P_a = 150$ mmHg.

simulated with the given data of Waschke *et al.* [25]. The mean arterial blood pressure P_a was decreased linearly to 86, 70, 55 and 40 mmHg and the cerebral blood flow under these conditions was calculated after another period of 1 h 25 min.

Figure 17 shows the dependence of cerebral blood flow on mean arterial blood pressure in the situation of brain damage described above. The calculated lower autoregulation limit increased from $40 < x < 55$ mmHg under basal conditions to $70 < x < 86$ mmHg. Engelborghs *et al.* [28] measured a lower autoregulation limit of 46.9 ± 12.7 in sham rats and 62.2 ± 20.8 in CHI rats.

In figure 18 the effect of L-NAME infusion on blood flow in the rat cerebral cortex is shown. Hudetz *et al.* [29] measured the laser-Doppler flow (LDF) thirty minutes after N^ω-nitro-L-arginine methyl ester (L-NAME) administration (20 mg/kg). LDF was reduced from 159 ± 14 to 135 ± 11 perfusion units (PU) (15% decrease), whereas

mean arterial pressure P_a was increased from 105 ± 4 to 132 ± 6 mmHg (26% increase).

This effect of nitric oxide inhibition is numerically simulated in the way that the following parameters are changed linearly in thirty minutes: the basal value of blood pressure $P_a = 116$ mmHg is increased to 146.16 mmHg (26% increase) and the basal NO production rate $q_{NO} = 54.1$ ng/g tissue is decreased to 5.4 ng/g tissue (90% decrease). The cerebral blood flow was calculated after another period of thirty minutes and it was decreased from 0.1696 to 0.1393 ml s⁻¹ (17.8% decrease).

6. Discussion

In this paper, a mathematical model is presented which describes cerebral hemodynamics under physiological aspects. The overall aim is to develop a tool that provides a more complete insight into the mechanisms of cerebrovascular perfusion with special emphasis of the interaction of different regulatory mechanisms. To facilitate hypothesis testing in the lab a species specific model using data from the Sprague-Dawley rat was developed. In the first instance, only two of the most robust mechanisms have been integrated into the model: CO₂- and NO-regulation.

By introducing a cardiac output function as input for the systemic blood circulation the blood pressure gets dependent on time and thus all pressures of the model and the blood flow become pulsatile. The implementation of pulsatile blood flow allows to investigate the effects of cardiac dysrhythmias on cerebral perfusion which is an important problem with respect to the increasing population of elderly trauma victims with cardiac comorbidities. The systemic circulation is closed for the first time in this model, so all changes in cardiac output result in changes of other systemic pressures and flows.

Maintenance of an adequate cerebral perfusion pressure is a mainstay of TBI (traumatic brain injury)

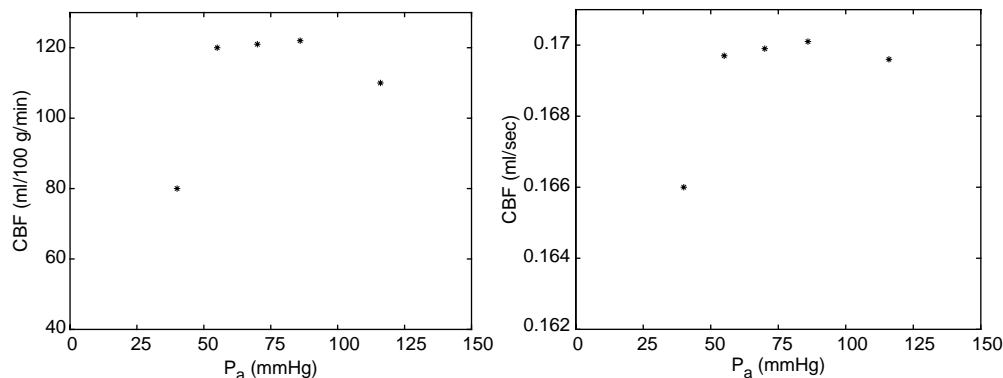


Figure 15. Left: measured data of Waschke *et al.* [25]: the mean arterial blood pressure P_a is reduced from 116 to 86, 70, 55 and 40 mmHg and the mean cerebral blood flow is measured for the corresponding pressure values in ml/100 g/min. Right: calculated mean cerebral blood flow for the given blood pressure values by the model. The changes in CBF depending on changes in blood pressure are qualitatively the same and it can be seen that the lower autoregulation limit must be in the range of 40 and 55 mmHg.

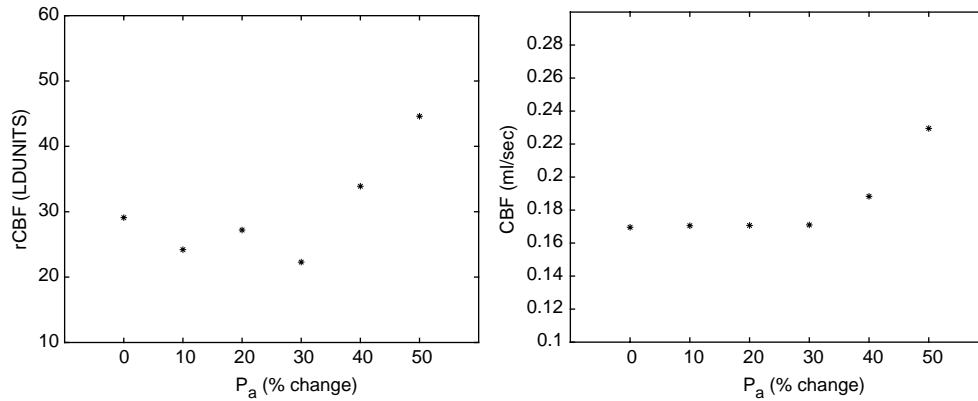


Figure 16. Left: measured data of Schaller *et al.* [26]: The mean arterial blood pressure P_a is raised up to 10, 20, 30, 40 and 50 percent of its basal value (116 mm Hg) and the mean regional cerebral blood flow is measured for the corresponding pressure values in LD-Units. Right: calculated mean cerebral blood flow for the given blood pressure values by the model. The increase in cerebral blood flow if blood pressure is increased up to 40 and 50% of its basal value is qualitatively the same and therefore the upper regulation limit must be in the range of 150 and 160 mm Hg.

therapy and is thought to be a necessary and potentially neuroprotective therapeutic intervention that “may be associated with a substantial reduction in mortality and improvement in quality of survival and is likely to enhance perfusion to ischemic regions of the brain after severe TBI” (cf. [30]). This goal can be reached by intravenous application of vasopressors (e.g. norepinephrine). The immediate effector organ of vasopressors is the heart where an increase of cardiac output results from modulation of heart rate and contractility. Interestingly there appears to be a feedback from TBI to cardio-circulatory performance in terms of a reduced response to vasopressors under certain conditions (cf. [22]). Thus, the system of sympathetic regulation of heart function needs to be implemented into a physiologically relevant model of cerebral perfusion. In the present version of the model only the very basic

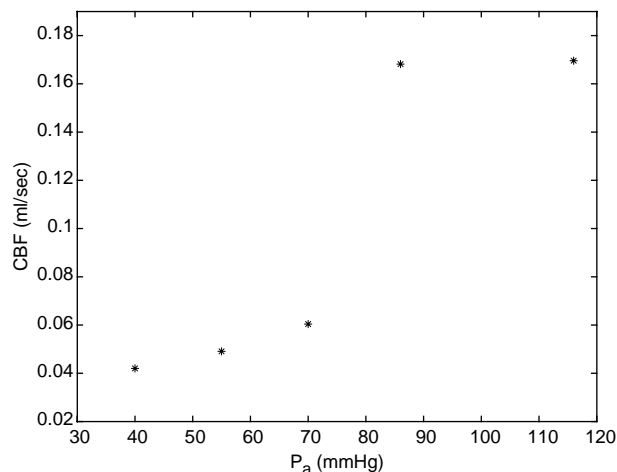


Figure 17. Numerically simulated dependence of CBF on mean arterial pressure under the situation of a head injury. The values of the intracranial pressure, P_{aCO_2} and b under this condition are given by [27] and [25], respectively. The lower autoregulation limit increased and lies in the range of $70 < x < 86$ mm Hg.

mechanism of norepinephrine physiology was considered as the model is focused only on the most basic and robust mechanisms of cerebral perfusion (flow, autoregulation). After the fundamental behaviour of cerebral blood flow has been successfully modelled future versions of the model need to map the effects of vasopressors more precisely.

Other important features of the model are the regulation mechanisms, like autoregulation, CO_2 = reactivity and NO reactivity, which regulate the cerebral blood flow under changes in arterial CO_2 pressure, endothelial NO production and changes in CBF itself.

Several considerations are made to extend the model in the following way: the point of extension deals with the assumptions which are made for NO reactivity. It is important to note that NO is also produced at other regions in brain and thus has an effect on the smooth muscle cells of, i.e. large cerebral arteries and veins, and yields a change in compliance and resistance of these vessels. There is also a change in stroke volume ν , heart rate b and systemic resistance R_s as a consequence of NO production at the vessel cells of central veins (i.e. vena cava), which has to be taken into account. However, NO is treated as an input quantity of the system. This means that the distinct sources of NO generation have not been modelled explicitly. A thorough model of NO generation needs to comprise a variety of cell types (endothelial cells, astrocytes, etc.) as well as a complicated system of subcellular structures. Thus the simplification of NO physiology, i.e. to consider NO “to be simply there”, appears justified. A multiscale submodel of NO physiology would complicate the model as a whole substantially. A multiscale submodel would only be justified in terms of additional information if a spatial resolution of the cerebrovascular system were given as these subcellular events are governed by the local milieu. In the present model, variation of NO concentrations within physiologic bounds will provide the necessary information.

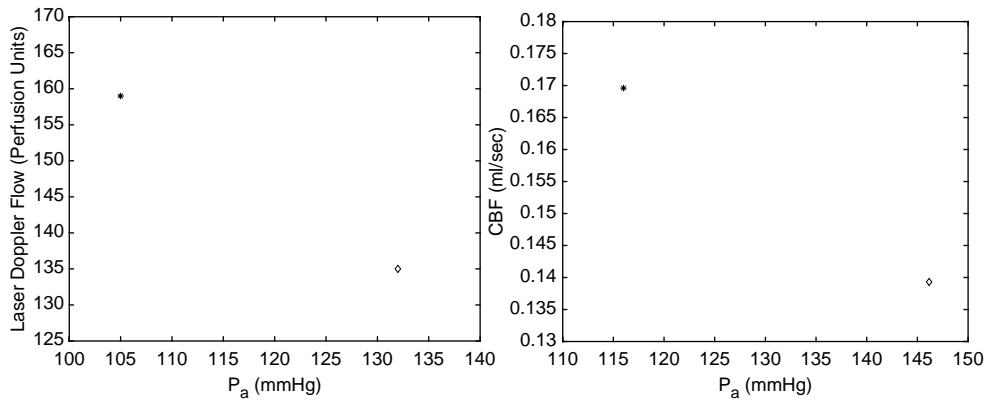


Figure 18. Left: measured data of Hudetz *et al.* [29], which show the effects of nitric oxide synthase inhibition with L-NAME on mean laser-Doppler flow and mean arterial pressure P_a in rat cerebral cortex. *, control; ◇, L-NAME. Right: numerically simulated effect of L-NAME infusion and increased blood pressure P_a on CBF. The 26% increase in blood pressure and the 90% decrease in NO production rate yield an 17.8% decrease in CBF in comparison to the 15% decrease measured by Hudetz *et al.* [29].

References

- [1] Ursino, M. and Lodi, C.A., 1998, Interaction among autoregulation, CO₂ reactivity, and intracranial pressure: a mathematical model, *American Journal of Physiology: Heart and Circulatory Physiology*, **274**, H1715–H1728.
- [2] Ursino, M., Ter Minassian, A., Lodi, C.A. and Beydon, L., 2000, Cerebral hemodynamics during arterial and CO₂ pressure changes: *in vivo* prediction by a mathematical model, *American Journal of Physiology: Heart and Circulatory Physiology*, **279**, H2439–H2455.
- [3] Ursino, M. and Lodi, C.A., 1997, A simple mathematical model of the interaction between intracranial pressure and cerebral hemodynamics, *Journal of Applied Physiology*, **82**(4), 1256–1269.
- [4] Olufsen, M.S., Nadim, A. and Lipsitz, L.A., 2002, Dynamics of cerebral blood flow regulation explained using a lumped parameter model, *American Journal of Physiology: Regulatory Integrative and Comparative Physiology*, **282**, R611–R622.
- [5] Molino, P., Cerutti, C., Julien, C., Cuisinaud, G., Gustin, M.-P. and Paultre, C., 1998, Beat-to-beat estimation of windkessel model parameters in conscious rats, *American Journal of Physiology*, **274**, H171–H177.
- [6] Stevens, S.A., Lakin, W.D. and Goetz, W., 2003, A differentiable, periodic function for pulsatile cardiac output based on heart rate and stroke volume, *Mathematical Biosciences*, **182**(2), 201–211.
- [7] Harper, S.L., Bohlen, H.G. and Rubin, M.J., 1984, Arterial and microvascular contributions to cerebral cortical autoregulation in rats, *American Journal of Physiology*, **246**, H17–H24.
- [8] Muir, J.K. and Ellis, E.F., 1993, Cocaine potentiates the blood pressure and cerebral blood flow response to norepinephrine in rats, *European Journal of Pharmacology*, **249**(3), 287–292.
- [9] Iadecola, C., 1992, Does nitric oxide mediate the increases in cerebral blood flow elicited by hypercapnia?, *Proceedings of the National Academy of Sciences USA*, **89**(9), 3913–3916.
- [10] Malyshev, I.Y., Zenina, T.A., Golubeva, L.Y., Saltykova, V.A., Manukhina, E.B., Mikoyan, V.D., Kubrina, L.N. and Vanin, A.F., 1999, NO-Dependent mechanisms of adaptation to hypoxia, *Nitric oxide: Biology and Chemistry*, **3**(2), 105–113.
- [11] Yu, M., Sun, C.-W., Maier, K.G., Harder, D.R. and Roman, R.J., 2002, Mechanism of cGMP contribution to the vasodilator response to NO in rat middle cerebral arteries, *American Journal of Physiology: Heart and Circulatory Physiology*, **282**, H1724–H1731.
- [12] Arribas, S.M., Vila, E. and McGrath, J.C., 1997, Impairment of vasodilator function in basilar arteries from aged rats, *Stroke*, **28**, 1812–1820.
- [13] Wang, Q., Pelligrino, D.A., Baughman, V.L., Koenig, H.M. and Albrecht, R.F., 1995, The role of neuronal nitric oxide synthase in regulation of cerebral blood flow in normocapnia and hypercapnia in rats, *Journal of Cerebral Blood Flow and Metabolism*, **15**(5), 774–778.
- [14] Niwa, K., Lindauer, U., Villringer, A. and Dirnagl, U., 1993, Blockade of nitric oxide synthesis in rats strongly attenuates the CBF response to extracellular acidosis, *Journal of Cerebral Blood Flow and Metabolism*, **13**(3), 535–539.
- [15] Wang, Q., Pelligrino, D.A., Koenig, H.M. and Albrecht, R.F., 1994, The role of endothelium and nitric oxide in rat pial arteriolar dilatory responses to CO₂ *in vivo*, *Journal of Cerebral Blood Flow and Metabolism*, **14**, 944–951.
- [16] Harada, M., Fuse, A. and Tanaka, Y., 1997, Measurement of nitric oxide in the rat cerebral cortex during hypercapnoea, *NeuroReport*, **8**, 999–1002.
- [17] Muchitsch, E.-M., Pichler, L. and Schwarz, H.P., 2004, Effects of α 1-acid glycoprotein in combination with catecholamines on hemorrhagic hypovolemic shock in rats, *Arzneim-Forsch/Drug Research*, **54**(2), 95–101.
- [18] Mokrane, A. and Nadeau, R., 1998, Dynamics of heart rate response to sympathetic nerve stimulation, *American Journal of Physiology*, **275**, H995–H1001.
- [19] Gotoh, T.M., Fujiki, N., Tanaka, K., Matsuda, T., Gao, S. and Morita, H., 2004, Acute hemodynamic responses in the head during microgravity induced by free drop in anesthetized rats, *American Journal of Physiology: Heart and Circulatory Physiology*, **286**, R1063–R1068.
- [20] Baumbach, G.L., 1996, Effects of increased pulse pressure on cerebral arterioles, *Hypertension*, **27**, 159–167.
- [21] Sugiyama, T., Kawamura, K., Nanjo, H., Sageshima, M. and Masuda, H., 1997, Loss of arterial dilation in the reendothelialized area of the flow-loaded rat common carotid artery, *Arteriosclerosis Thrombosis and Vascular Biology*, **17**, 3083–3091.
- [22] Holtzer, S., Vigue, B., Ract, C., Samii, K. and Escourrou, P., 2001, Hypoxia-hypotension decreases pressor responsiveness to exogenous catecholamines after severe traumatic brain injury in rats, *Critical Care Medicine*, **29**(8), 1609–1614.
- [23] Mayhan, W.G. and Heistad, D.D., 1986, Role of veins and cerebral venous pressure in disruption of the blood-brain barrier, *Circulatory Research*, **59**, 216–220.
- [24] Hauerberg, J., Ma, X., Bay-Hansen, R., Pedersen, D.B., Rochat, P. and Juhler, M., 2001, Effects of alterations in arterial CO₂ tension on cerebral blood flow during acute intracranial hypertension in rats, *Journal of Neurological Anesthesia*, **13**(3), 213–221.
- [25] Waschke, K.F., Riedel, M., Lenz, C., Albrecht, D.M., von Ackern, K. and Kuschinsky, W., 2004, Regional heterogeneity of cerebral blood flow response to graded pressure-controlled hemorrhage, *Journal of Trauma*, **56**, 591–603.
- [26] Schaller, C., Nakase, H., Kotani, A., Nishioka, T., Meyer, B. and Sakaki, T., 2002, Impairment of autoregulation following cortical venous occlusion in the rat, *Neurological Research*, **24**, 210–214.

- [27] Engelborghs, K., Verlooy, J., Van Reempts, J., Van Deuren, B., Van de Ven, M. and Borgers, M., 1998, Temporal changes in intracranial pressure in a modified experimental model of closed head injury, *Journal of Neurosurgery*, **89**, 796–806.
- [28] Engelborghs, K., Haseldonckx, M., Van Reempts, J., Van Rossem, K., Wouters, L., Borgers, M. and Verlooy, J., 2000, Impaired autoregulation of cerebral blood flow in an experimental model of traumatic brain injury, *Journal of Neurotrauma*, **17**(8), 667–677.
- [29] Hudetz, A.G., Smith, J.J., Lee, J.G., Bosnjak, Z.J. and Kampine, J.P., 1995, Modification of cerebral laser-Doppler flow oscillations by halothane, P_{CO_2} , and nitric oxide synthase blockade, *American Journal of Physiology*, **269**, H114–H120.
- [30] The Brain Trauma Foundation, 2000, The American Association of Neurological Surgeons. The joint section on neurotrauma and critical care. Guidelines for cerebral perfusion pressure, *Journal of Neurotrauma*, **17**, 507–511.